

PACS numbers: 42.55.Px; 42.25.Kb; 42.25.Hz; 42.50.Nn
DOI: 10.1070/QE2012v042n12ABEH015031

Comparison of the coherence properties of superradiance and laser emission in semiconductor structures

P.P. Vasil'ev, R.V. Penty, I.H. White

Abstract. **The coherence properties of a transient electron–hole state developing during superradiance emission in semiconductor laser structures have been studied experimentally using a Michelson interferometer and Young's classic double-slit configuration. The results demonstrate that, in the lasers studied, the first-order correlation function, which quantifies spatial coherence, approaches unity for superradiant emission and is 0.2–0.5 for laser emission. The supercoherence is due to long-range ordering upon the superradiant phase transition.**

Keywords: *superradiance, coherence, semiconductor laser structures, Young's experiment, interference pattern.*

1. Introduction

A transition of an atomic, molecular or electron–hole system to quantum (condensed, superfluid or superconducting) phases is an extraordinary process where both the microscopic and macroscopic properties of the system undergo fundamental changes. Bose condensation, i.e. the accumulation of a macroscopically large number of particles in their ground energy state, has been demonstrated in a number of physical systems, including ultracold atomic gases and ensembles of quasiparticles in solids [1–5]. In some instances, the quantum state of matter is the result of equilibrium condensation. The most typical example is the superconducting state of Cooper pairs in metals. In many cases, however, the lifetime of particles or quasiparticles is finite and ranges from pico- to milliseconds. Even in such cases, condensation is possible provided the lifetime of the particles is much longer than the characteristic time of interparticle scattering. It is generally admitted at present that phase coherence over macroscopic distances is an inherent property of all Bose condensates [6, 7]. Experimental studies of interference between two condensates or between two parts of a given condensate are often thought to provide more convincing evidence in comparison with examination of a macroscopically large ground-state population [8]. The development of long-range order and spatial coherence can be measured using interference patterns obtained either with a Michelson interferometer or in Young's classic experiment.

Superradiance (SR) (collective spontaneous recombination) has many characteristics of a quantum phase transition [9, 10]. One of its key features is mutual phasing of the emitters involved, without which SR is essentially impossible [11]. A collective SR state in a medium implies the development of macroscopic polarisation, which suggests ordering. Following a detailed theoretical study [12], SR emission was found experimentally in many media: gases, solids and semiconductors, including quantum dot systems and exciton condensates at low temperatures [11, 13]. In semiconductors, SR emission was detected as high-power femtosecond pulses in multiple-section GaAs/AlGaAs laser structures in the late 1990s [14, 15]. The ability of such structures to generate conventional laser radiation along with SR suggested that the observed generation of femtosecond pulses might be the result of normal lasing. Subsequent experimental and theoretical studies [16–18] have clearly shown, however, that the characteristic features of SR emission differ radically from those of lasing. The dissimilarity originates from the fact that different states of the semiconductor underlie lasing and SR emission. The output of a semiconductor laser is coherent, whereas the semiconducting medium remains incoherent. In contrast, both the electromagnetic field and electron–hole system are coherent during SR generation.

In this paper, we present experimental data demonstrating that, during SR generation, the electron–hole system in the active region possesses spatial coherence in both the longitudinal and transverse directions, and that the degree of coherence in this state exceeds that of laser emission.

2. Experimental

We studied two types of GaAs/AlGaAs laser structures, differing in active layer configuration. The structures each consisted of three sections: two gain sections at their ends and an electrically controlled optical absorber in between. Figure 1 schematically shows a cross-sectional view of the active region of the semiconductor structures. A GaAs layer about 0.2 μm thick was sandwiched between a p- and an n-AlGaAs layer. Passing through the gain sections, nanosecond current pulses produced electron and hole concentrations from 10^{17} to 10^{19} cm^{-3}, depending on the amplitude of the current, I. A variable reverse bias, V, applied to the middle section was used to control the optical absorption in the active layer. Spontaneous emission and normal lasing were ensured by different values of I and V. For example, a typical threshold

P.P. Vasil'ev P.N. Lebedev Physics Institute, Russian Academy of Sciences, Leninsky prosp. 53, 119991 Moscow, Russia; Centre for Photonic Systems, Department of Electrical Engineering, University of Cambridge, 9 JJ Thomson Avenue, CB3 0FA, UK;
e-mail: pv261@cam.ac.uk;
R.V. Penty, I.H. White Centre for Photonic Systems, Department of Electrical Engineering, University of Cambridge, 9 JJ Thomson Avenue, CB3 0FA, UK

Received 24 October 2012
Kvantovaya Elektronika **42** (12) 1081–1086 (2012)
Translated by O.M. Tsarev

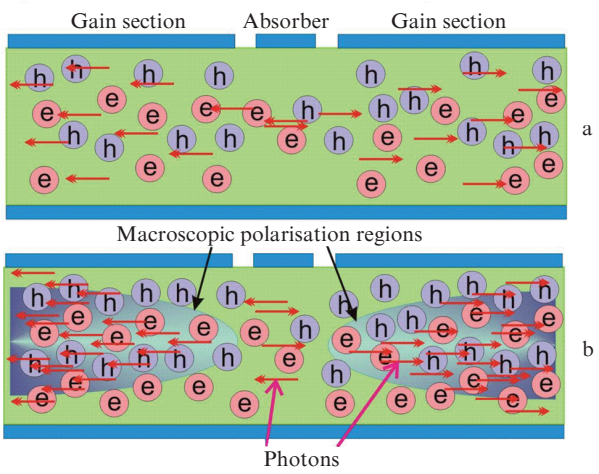

Figure 1. Schematic of the active layer: (a) lasing, (b) superradiant emission.

carrier concentration for lasing at $V = 0$ was $(1.0-1.5) \times 10^{18}$ cm^{-3}. The parameters of the laser structures were reported elsewhere [11, 16, 17].

Because of the different ultrafast relaxation processes in the semiconductor (electron – electron and electron – hole collisions and interactions with phonons), the electron – hole pairs (quantum emitters) in it are incoherent with each other. Typical room-temperature polarisation relaxation times are 10^{-14} to 10^{-13} s, so there is no macroscopic polarisation and no ordered state in the laser system. Increasing the bias V increases the absorption and can prevent lasing. As shown earlier [11], the SR state may develop in the active layer at rather high I and V. Conditions for the formation of this state and the underlying mechanism were investigated previously [11, 16–18]. Typical carrier concentrations in this state exceed 6×10^{18} cm^{-3}.

The coherence of the SR state can be assessed readily by analysing the output emission from the facets of the structure using a Michelson interferometer. We performed such an experiment with one type of laser structure, which had a rectangular active region 5–6 μm in width and 100 μm in total length. The absorber was 10 μm long, and the gain sections were 30 μm long. Our experimental data are presented in Section 3.

In addition, we measured the spatial coherence of the SR state in a transverse direction using the well-known Young's double-slit configuration [19], which has recently become a standard approach for demonstrating a long-range order and spatial coherence of condensed quantum states [20, 21]. The measurements were made using the other type of semiconductor structure, which had a waveguide geometry with the active layer width increasing from 5 to 30–40 μm, depending on the sample. Figure 2 shows a schematic of our experimental setup. Interference patterns of the light emitted by a semiconductor structure and passed through two slits were observed using a CCD video camera in the spontaneous emission, lasing and SR regimes. Since these regimes differ greatly in emission intensity, a variable optical attenuator was used to ensure that the camera had a linear response. In our experiments, we employed three double slits of different widths (5, 10 and 15 μm), with a separation between the slits, r, from 5 to 200 μm. The visibility of an interference pattern characterises the phase coherence between two points in the emitting region

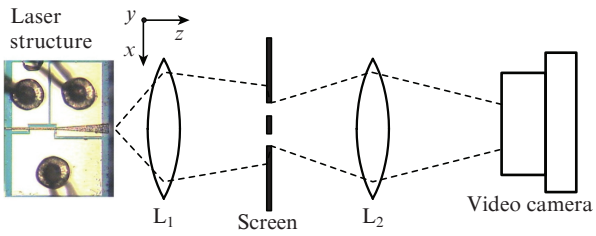

Figure 2. Schematic of Young's experiment with a tapered-waveguide semiconductor laser structure. The interference pattern is recorded with a CCD video camera. Lens L_1 projects the image of the emitting area onto the screen, and lens L_2 projects the image onto the image-receiving surface of the video camera.

of the structure. The evolution of the phase coherence in a semiconductor under various dynamic conditions can be assessed quantitatively by analysing the first order correlation function $g^{(1)}(r)$. The experimental data are presented in Section 4.

3. Coherence of a medium along its longitudinal axis

The first series of measurements were carried out with a Michelson interferometer that was used earlier to measure the femtosecond SR pulse duration in second harmonic generation [22]. Scanning the interferometer arm with micron accuracy allows one to assess the phase coherence of the radiation of interest. It is well known that the interferogram of any laser output has a single peak, located at zero delay. Its width is determined by the coherence time of the laser radiation and is inversely proportional to its spectral width. Two situations are possible in a multimode laser. One situation occurs when its modes are not phase-coupled (no mode locking). Interference is then observed only at zero delay in the interferometer arms, in a range determined by the spectral bandwidth. In the other situation, in the mode-locking regime, there are additional identical interference peaks separated by the round-trip time of the laser cavity [22]. Figure 3 shows typical second-order autocorrelation traces for laser emission and SR pulse generation in the first type of structure.

As expected, there is only one peak in the case of lasing, whereas the autocorrelation trace of SR emission at nonzero delays has several peaks and interference fringes. The only peak, at zero delay, in the case of laser emission is the result of incoherent amplification in the active medium of the laser. Indeed, electron – hole pairs remain coherent with the travelling resonant electromagnetic wave over a time determined by the relaxation time T_2. The many ultrafast relaxation processes in semiconductors lead to rapid coherence degradation, and the electrons and holes 'forget' the phase of the electromagnetic field and their own phases. In any laser, the medium remains incoherent, whereas the electromagnetic field is coherent. (Note that coherent media can be created in a time $\sim T_2$ by resonant pumping.) In the case under consideration, one can observe interesting coherent effects: photon echo, self-induced transparency, π and 2π pulse generation and others [23].

The correlation trace of SR in Fig. 3 is easy to interpret if one takes into account that there are two macroscopically large coherent regions represented in Fig. 1. The correlations induced in the electron – hole system in the early stages of the SR state, collective photon-mediated electron – hole pairing

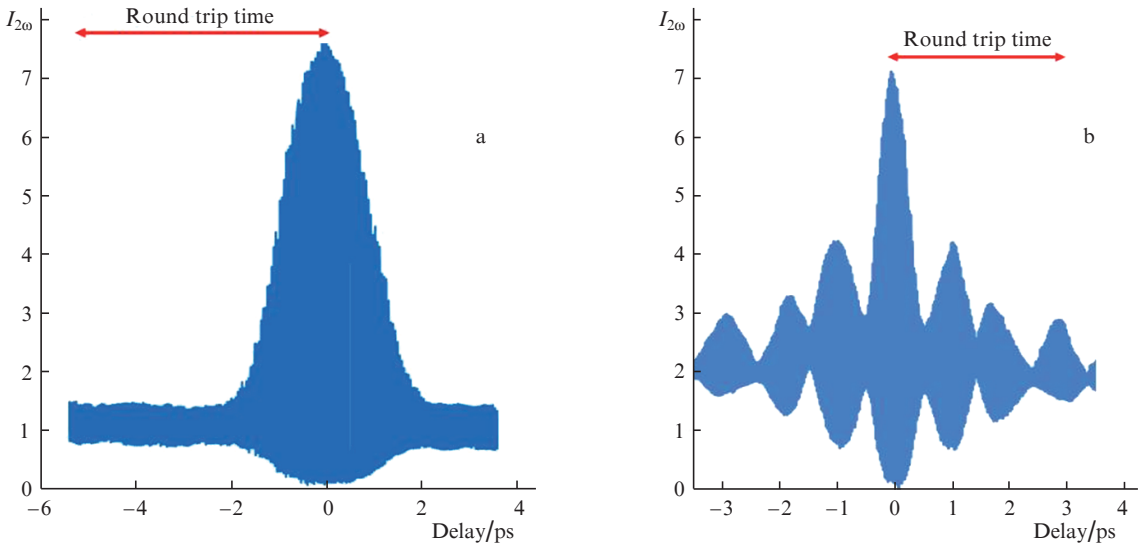

Figure 3. Second-order correlation traces, $I_{2\omega}$, for (a) laser emission and (b) superradiance.

and condensation on the band bottom result in a coherent BCS-like state, as described elsewhere [16–18]. Radiation emitted from a particular region in this state can be absorbed and then re-emitted in another region. The interference fringes seen in Fig. 3 during twice the round trip time indicate that the electron–hole system has extended spatially coherent regions. The multiple peaks in Fig. 3 arise from oscillatory energy exchange between the electromagnetic field and resonant semiconducting medium, similar to Bloch oscillations in a two-level system. In conclusion, note that the correlation trace in Fig. 3b is unique to SR emission. Semiconductor lasers have no such correlation traces in any other operation modes.

4. Spatial coherence in a transverse direction and Young's experiment

To more clearly demonstrate supercoherence in the SR regime, considerably exceeding the coherence of laser radiation, the following experiments were performed: We used spatially multimode semiconductor structures having a tapered waveguide (second type). Before carrying out Young's experiment with these emitters, we studied near-field lasing and SR emission dynamics using an electron-optical camera (streak camera) [11]. It is well known that strong optical nonlinearities in semiconductors may give rise to a variety of nonlinear optical phenomena, including self-focusing, wave front conjugation and Raman scattering. Spatial instability of the optical field in the active region of lasers, especially at a large width of the active region, leads to filamentation of the near-field emission pattern. The reasons for this are that individual spatial modes are independent and that the active medium is spatially incoherent. Near-field inhomogeneities, instability and filamentation of laser emission were observed in all our experiments with tapered-waveguide structures in the lasing regime.

It is well seen in Fig. 4 that the laser intensity varies strongly in space and time. In contrast, SR pulses are always generated simultaneously from the entire aperture of the laser structure. The results below demonstrate that the degree of spatial coherence in the SR state exceeds that of the laser radiation from the same spatially multimode structures. Figure 5 shows two series of images obtained in Young's experiment for laser radiation and SR emission. Regardless of experimental conditions, the visibility of the fringes for the superradiant emission is seen to be markedly better than that for lasing. The difference in the visibility of the interference patterns reflects the difference in phase coherence.

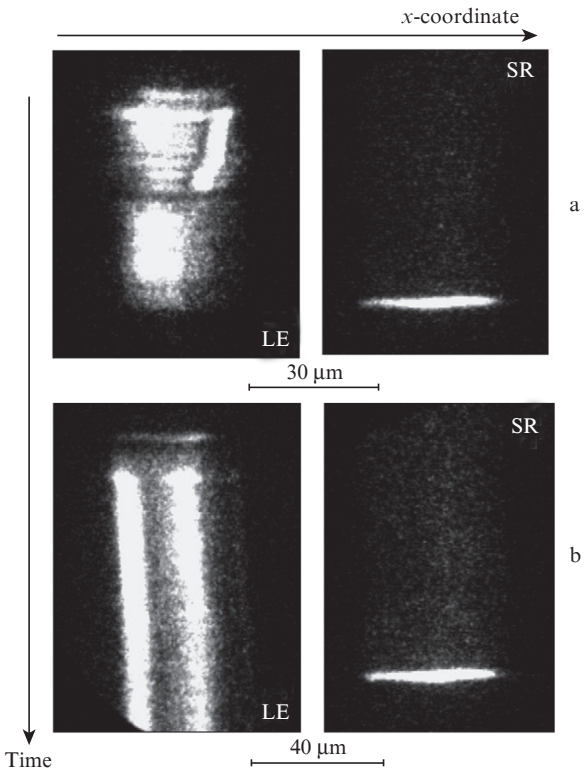

Figure 4. Near-field dynamics of laser emission (LE) and superradiance (SR) in two tapered-waveguide structures with an aperture of (a) 30 and (b) 40 μm.

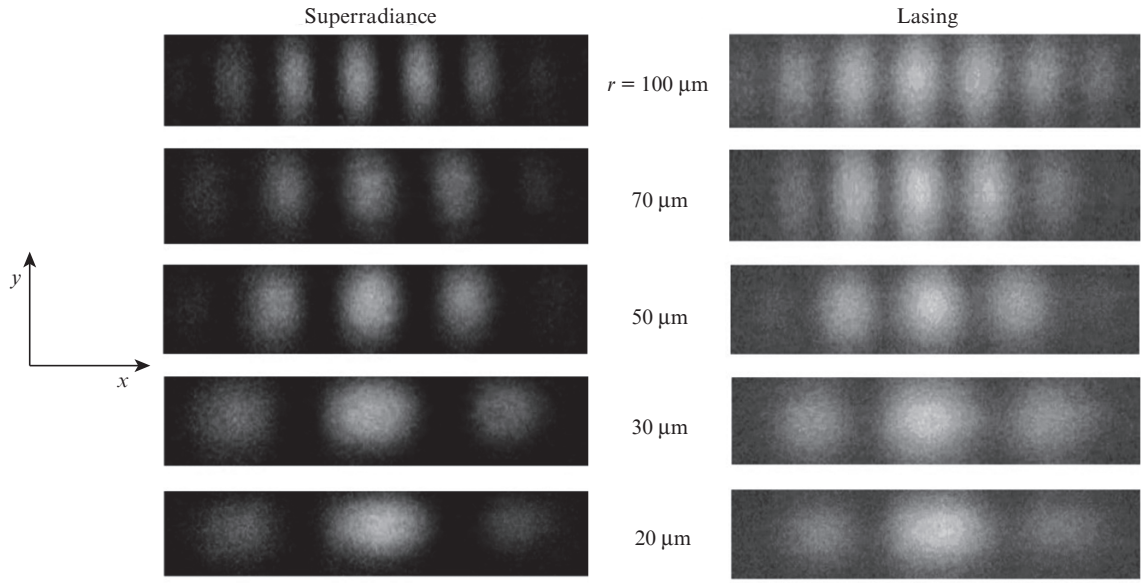

Figure 5. Interference patterns for lasing and superradiance at different slit separations.

The first-order spatial correlation function $g^{(1)}(r)$ quantifies the long-range order in quantum condensed states [3, 7, 20]. In addition, it is often thought of as the degree of condensation in phase space [20]. In our case, the correlation function $g^{(1)}(r)$ can be determined experimentally by analysing the visibility of the interference patterns in Fig. 5. To find $g^{(1)}(r)$, we integrate the image intensity $I(x, y)$ over a narrow strip along the y axis and fit the result with a theoretical dependence along the x axis. As is well known [24], the intensity of a double-slit interference pattern includes an oscillating term multiplied by a function of the form $\sin(x)/x$:

$$I(x) = I_1(x) + I_2(x) + 2g^{(1)}(r)\sqrt{I_1 I_2}\cos(\varphi(x) + \varphi_{12}), \qquad (1)$$

where

$$I_{1,2} = |E_{1,2}|^2 \operatorname{sinc}^2\left(\frac{x - x_0 \pm d/2}{X}\right); \quad \varphi(x) = \frac{2(x - x_0)}{X_c}; \qquad (2)$$

$$X = \frac{2D}{k\delta}; \quad X_c = \frac{2D}{kd}.$$

Here, d is the distance between the two slit images projected by lens L_2 onto the image plane; D is the spacing between this plane and the plane of the video camera; δ is the size of the slit image; x_0 is the coordinate of the centre of the two slits in the plane of the camera; I_1 (I_2) is the intensity of the image of one slit when the other is shut; and φ_{12} and $\varphi(x)$ are the constant and variable phases of the optical field in the plane of the camera. The parameters d, X and X_c were evaluated from experimental data, whereas $g^{(1)}(r)$, I_1, I_2, φ_{12} and $\varphi(x)$ were fitting parameters. The geometric parameters d, D, x_0 and δ; the parameters I_1, I_2, φ_{12} and $\varphi(x)$; and the fitting procedure were described elsewhere [21]. Figure 6 presents measurement results and the $I(x)$ curves obtained using Eqns (1) and (2).

The experimental data are seen to be well represented by the best fit curves. The only discrepancy occurs in the wings of the $I(x)$ for lasing. This may be due to the strong inhomogeneities of the near- and far-field laser radiation distributions, whereas Eqns (1) and (2) are, strictly speaking, valid only for the ideal case of a uniform field distribution. This is supported by the $I(x)$ fitting results for SR, which was always closer to a real situation (Fig. 6, right-hand panels). We carried out measurements for the tapered-waveguide structures with 30- and 40-μm output apertures under various driving conditions. The $g^{(1)}(r)$ calculation results are presented in Fig. 7.

There is a large difference between the data for SR and lasing. The partial spatial coherence in the case of lasing can be accounted for by the presence of several transverse modes in the spatial profile at all pumping levels and by the temporal and spatial instabilities of the emission in Fig. 4. In contrast to that of laser emission, the correlation function $g^{(1)}(r)$ of the superradiant state approaches unity at all slit widths and separations. Note that the condition $g^{(1)}(r) \sim 1$ is satisfied for any coherent condensed state with long-range order [3, 7, 20].

Attention should be paid to a very important fact. Spatial coherence with $g^{(1)}(r)$ approaching unity can be achieved in a single-mode laser, but coherence in a laser results from stimulated emission and the optical feedback from the laser cavity. Analysis of the evolution of spatial and temporal coherence in a laser demonstrates how coherent emission emerges from random spontaneous noise during wave amplification when light bounces back and forth between the mirrors. Coherence buildup requires hundreds and thousands of round trips in the cavity, the active medium being incoherent throughout.

In the case of SR, the observed $g^{(1)}(r) \sim 1$ is due to a different mechanism. The spatial coherence in both longitudinal and transverse directions is the result of self-organisation in the electron–hole system. Stimulated emission plays an important role in the development of correlation and ordering of the electron–hole system in the early stages of the evolution of the SR state [11, 17]. Nevertheless, the observed interference pattern is due to the coherence and long-range order (macroscopic polarisation) in the semiconductor and not to optical feedback. A macroscopically large number of carriers ($\sim 10^8$ pairs [11]), which occupy a significant part of the structure, recombine simultaneously. The typical duration of SR pulses generated by the structures studied here is within 1 ps, whereas the cavity round trip time exceeds 12 ps. This means that, in contrast to lasing, optical feedback plays no role in SR pulse generation and that the spatial coherence

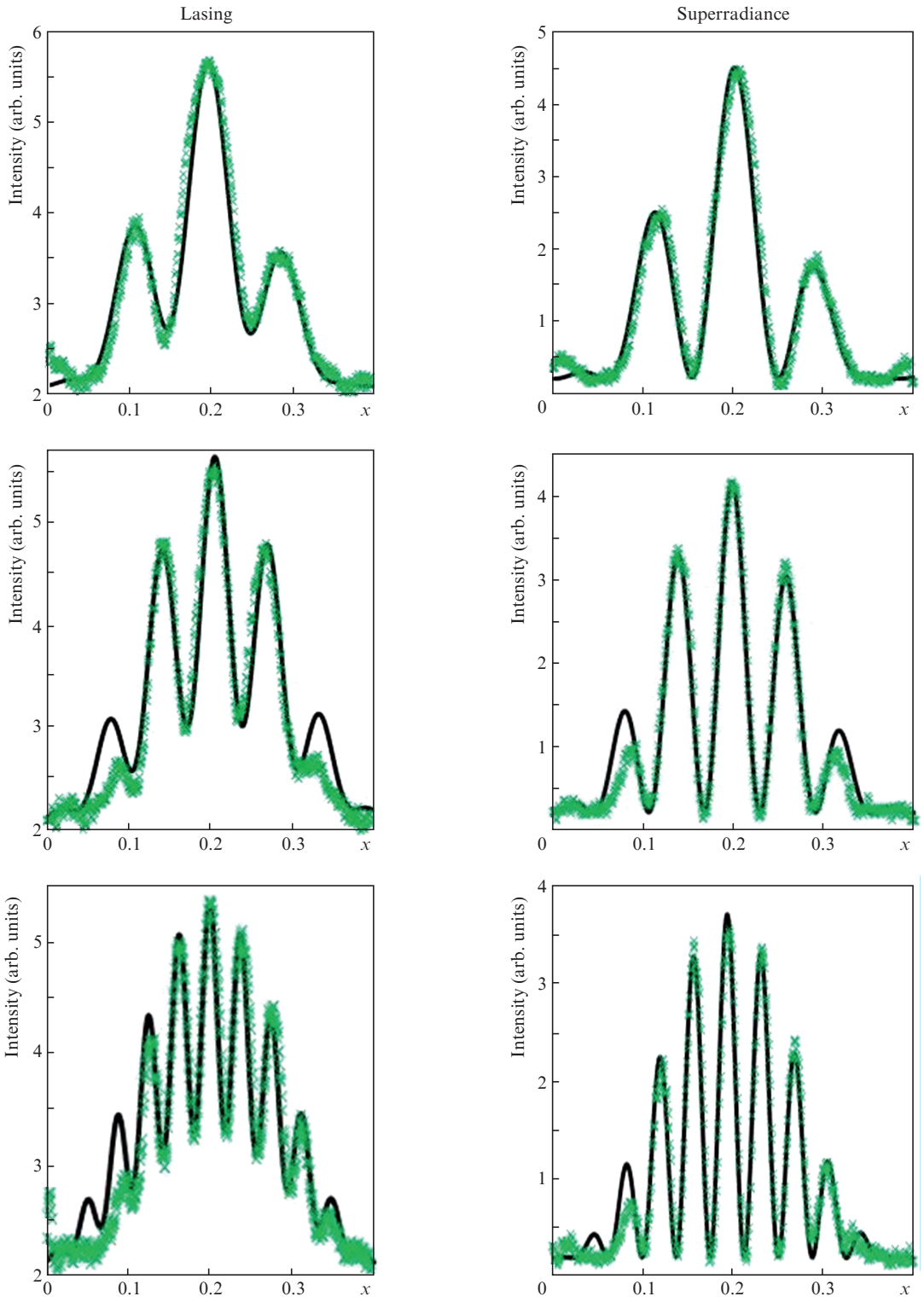

Figure 6. Interference functions $I(x)$ for lasing and superradiance emission. The points represent the experimental data and the solid lines represent the fits with Eqns (1) and (2).

observed in our experiments develops instantaneously and is only due to the coherence of the semiconductor.

5. Conclusions

The present experimental data demonstrate spatial coherence and macroscopic order in the high-density electron–hole system of GaAs laser structures during the generation of SR pulses at room temperature. The development of spatial coherence and long-range order was observed in both longitudinal and transverse directions with a Michelson interferometer and in Young's classic experiment. The first-order spatial correlation function $g^{(1)}(r)$, which quantifies long-range order, was shown to approach unity for the SR state, whereas $g^{(1)}(r) = 0.2-0.6$ for lasing in the same structures. The higher degree of coherence of the SR state is due to the spatial

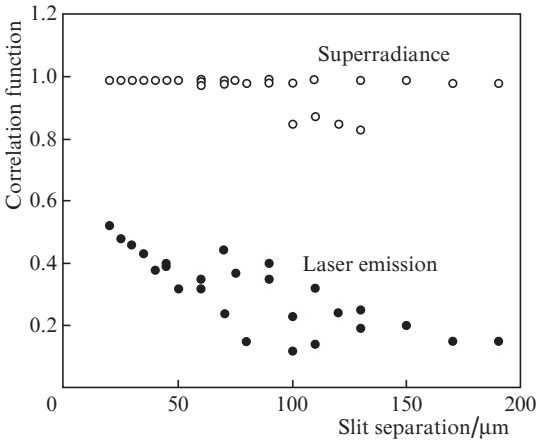

Figure 7. First-order correlation function $g^{(1)}(r)$ for SR emission and lasing.

coherence of the semiconductor. The present results provide additional evidence in favour of the formation of a nonequilibrium BCS-like coherent state in GaAs during a superradiant phase transition [11, 16–18].

Acknowledgements. This research was supported by the UK Engineering and Physical Science Research Council. We are grateful to V. Olle for fabricating the slit samples and to H. Kan and H. Ohta for producing the semiconductor structures.

References

1. Anderson M.H. et al. *Science*, **269**, 198 (1995).
2. Davis K.B. et al. *Phys. Rev. Lett*., **75**, 3969 (1995).
3. Deng H. et al. *Science*, **298**, 199 (2002).
4. Kasprzak J. et al. *Nature*, 443, 409 (2006).
5. Demokritov S.O. et al. *Nature*, **443**, 430 (2006).
6. Snoke D. *Nature*, **443**, 403 (2006).
7. Ritter S. et al. *Phys. Rev. Lett*., **98**, 090402 (2007).
8. Dicke R.H. *Phys. Rev*., **93**, 99 (1954).
9. Wang Y.K., Hioe F.T. *Phys. Rev. A*, **7**, 831 (1973).
10. Baumann K. et al. *Nature*, **464**, 1301 (2006).
11. Vasil'ev P.P. *Rep. Prog. Phys*., **72**, 076501 (2009).
12. Gross M., Haroche S. *Phys. Rep*., **93**, 301 (1982).
13. Andreev A.V. et al. *Cooperative Effects in Optics: Superradiance and Phase Transitions* (Bristol: IOP Publishing, 1993).
14. Vasil'ev P.P. *Kvantovaya Elektron*., **24** (10), 885 (1997) [*Quantum Electron*., **27** (10), 860 (1997)].
15. Vasil'ev P.P. *Kvantovaya Elektron*., **29** (1), 4 (1999) [*Quantum Electron*., **29** (10), 842 (1999)].
16. Vasil'ev P.P. et al. *Phys. Rev. B*, **64**, 195209 (2001).
17. Vasil'ev P.P. *Phys. Status Solidi B*, **241**, 1251 (2004).
18. Vasil'ev P.P. *Phys. Rev. B*, **74**, 125206 (2006).
19. Young T. *Philos. Trans. R. Soc. London*, **94**, 1 (1804).
20. Bloch I. et al. *Nature*, **403**, 166 (2000).
21. Deng H. et al. *Phys. Rev. Lett*., **99**, 126403 (2007).
22. Vasil'ev P. *Ultrafast Diode Lasers: Fundamentals and Applications* (Norwood: Artech House, 1995).
23. Allen L., Eberly J.H. *Optical Resonance and Two-level Atoms* (New York: Wiley, 1975).
24. Born M., Wolf E. *Principles of Optics* (Oxford: Pergamon, 1969; Moscow: Nauka, 1970).